Feng, Z., Long, Z., and Chen, Q. 2014. "Assessment of various CFD models for predicting airflow and pressure drop through pleated filter system," *Building and Environment*, 75, 132-141.

Assessment of various CFD models for predicting airflow and pressure drop through pleated filter system

Zhuangbo Feng[1], Zhengwei Long[1, *], Qingyan Chen[2, 1]

[1] *School of Environmental Science and Engineering, Tianjin University, Tianjin 300072, China*

[2] *School of Mechanical Engineering, Purdue University, West Lafayette, IN 47907, USA*

Abstract

Pleated filters, sometimes in combination with an electrostatic precipitator, are widely used to control particle contaminants in enclosed environments. Such a filter system can improve the health of occupants in these spaces. Computational Fluid Dynamics (CFD) can be a powerful tool for optimizing the design of pleated filter system. However, the performance of various CFD models has not been clearly understood for predicting transitional turbulent flows in pleated filter systems. This study evaluated the performance of several turbulence models, including the standard *k-ε* model, low Reynolds number *k-ε* models, the v2f model, Large Eddy Simulation (LES) models, and Detached Eddy Simulation (DES) models, for simulating the pressure drop and transitional flows through pleated filters both with and without an electrostatic precipitator. The simulated results from the models were compared with the experimental data from the literature and our measurements. The results indicate that the v2f, LES and DES (Spalart–Allmaras) can accurately predict the pressure drop and flow distributions in pleated filters. Because the LES requires high computing capacity and speed, the DES (Spalart–Allmaras) and the v2f models are recommended for the optimal design of a pleated filter system.

Keywords: Particulate; pleated filter; electrostatic precipitator; transitional flow; CFD

Introduction

Most people spend 90% of their time in enclosed environments such as buildings, cars, and public transportation. Particulates exist in these environments, and the health of occupants is related to particulate concentration (Chio and Liao, 2008), as in the cases of children's atopic dermatitis (Song et al., 2011) and lung cancer (Pope et al., 2002). Sometimes the particulates contain various types of bacteria and viruses that cause infectious diseases. These airborne particulates can create a very high risk for occupants (Mangili and Gendreau, 2005). Hence, the control of indoor airborne particles is very important.

Many technologies, including pleated filters and electrostatic precipitators, are available for removing air particles. Pleated filters, such as High-Efficiency Particulate Air (HEPA) filters, are widely used in buildings and airplanes. Properly maintained HEPA filters can remove at least 99.97% of airborne particles with a diameter of 0.3 micrometers or larger (Hocking, 2000). However, this type of filter has a limited working life because the pressure drop across it increases during the particle collection process. An increase in the pressure drop causes an increase in energy consumption by the fan, so that it is necessary to change the filter periodically. In addition, the particle layer on the surface of pleated filters may pollute the air (Clausen, 2004). Electrostatic precipitators (ESPs) collect the particles by use of an electric field. ESPs have a low pressure drop but also a low collection efficiency for submicron particles (Morawska et al., 2002). Therefore, hybrid filtering systems combining the two technologies have been developed to make use of their respective strengths. Croxford et al. (2000) found that a local ESP with a front pre-filter could significantly reduce the concentration of indoor airborne particles, especially for small particles. Skulberg et al. (2005) experimentally studied the performance of a hybrid local ESP and carbon filter system in an

office and found that this system could significantly reduce the indoor particle concentration. Zuraimi and Tham (2009) measured the particle concentration in an office building equipped with an ESP with a Pre-Filter (ESP-PF); they found that the hybrid system worked very well. The removal efficiency of the ESP-PF filter was close to 100% for particles with a diameter larger than 0.3 μm. Huang et al. (2008) developed an enhanced low-efficiency filter with an air ion emitter to reduce the concentration of biological particles in a heating, ventilating, and air-conditioning (HVAC) system. Park et al. (2009, 2011) developed a carbon fiber ionized-assisted filter to improve the removal efficiency for submicron aerosol particles and bioaerosols in an HVAC system. These studies demonstrated the advantages of technologies that combine the ESP and pleated filters. As pleated filter systems become more and more complicated, it becomes challenging to create an optimization design.

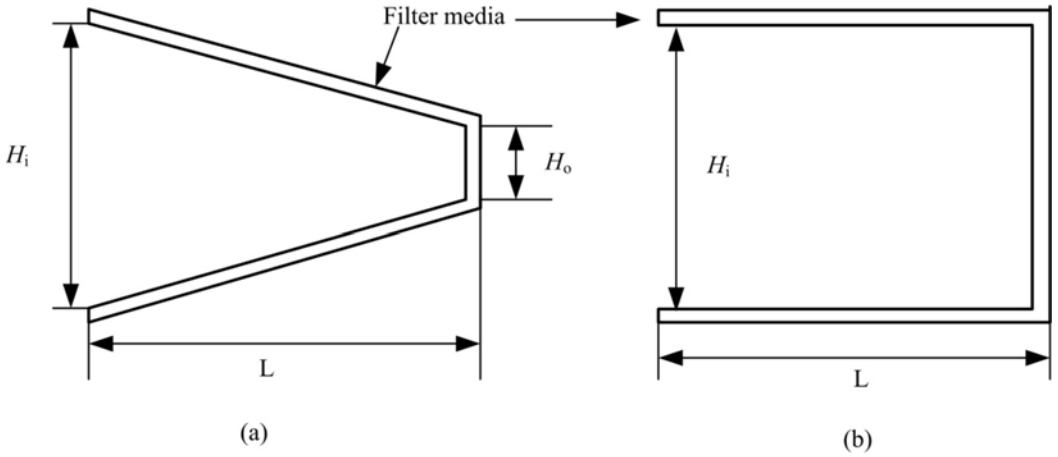

Fig. 1. The structures of pleated filters: (a) trapezoidal type; (b) rectangular type

Numerical methods have been developed over the years for the optimization design of the ESP (Gallimberti, 1998), pleated filters (Chen et al., 1995; Subrenat et al., 2003; Rebai et al., 2010; Fotovati et al., 2011, 2012) and hybrid systems (Long and Yao, 2012). The most important aspect of the optimization design is to determine the flow field through the filter systems. The flow pattern in the ESP is fully turbulent with a high Reynolds number, and many turbulence models can be used as recommended by Kallio and Stock (1992) and Schmid et al. (2002). However, simulations of the flow field through a pleated filter are more difficult. Figure 1 shows the structures of two types of pleated filter. In the ducts of common HVAC systems, the upstream air flow of the pleated filter is usually fully developed (Liu et al., 2012). But the flow in the porous media of the air filter is laminar (Rebai et al., 2010; Fotovati et al., 2011). The flow in the air channel of the pleated filter changes from the turbulent flow to the laminar flow. Therefore, the air flow through the pleated air filter is very complex and a combination of the three basic types of the air flow: turbulent, laminar and transitional. Many semi-empirical models are available for predicting the flow field and pressure drop through a fiber or a flat filter. For example, Feng (2007) derived an analytical method by using Darcy's law for predicting pressure drop through a pleated filter, and the results matched the experimental data well. However, such a model assumes a uniform filtration velocity distribution along the surface of the filter media, which may not be accurate. Rebai et al. (2010) developed a semi-analytical model for simulating the flow field in pleated filters, which could predict both the pressure drop and the gas filtration velocity. However, their model provides only the one-dimensional velocity and does not account for the full details of the flow field information. As flow through a filter is governed by the Navier–Stokes equations, the Computational Fluid Dynamics (CFD)

technique has also been used to predict the performance of pleated filters. Chen et al. (1995) used the laminar flow model to optimize pleated filters with a finite element method. Subrenat et al. (2003) studied three-dimensional flow in a cylindrical pleated filter by solving the time-averaged Navier–Stokes equations combined with the standard k-ε turbulence model (Launder and Splading, 1974), and the results matched the experimental pressure drop data. Rebai et al. (2010) used a laminar flow model to simulate the flow field in pleated filters for validating a semi-analytical model. Fotovati et al. (2011, 2012) used a laminar flow model combined with a particle collection model to simulate the instantaneous transitional flow field of pleated filters during a cake clogging process. Although the laminar flow model for flow simulation in pleated filters appears to be acceptable in the above applications, the flow through the pleated filter is actually not simple laminar. Especially in some hybrid systems (Croxford et al., 2000; Skulberg et al., 2005; Huang et al., 2008; Park et al., 2009, 2011), the gas flow is a combination of fully turbulent, transitional and laminar flow. Thus, a suitable model that can simulate the turbulence flow filed in the pleated filter system is necessary for the optimal design and performance analysis. Possible models include the Low Reynolds Number (LRN) k-ε models, Large Eddy Simulation (LES) models, and Detached Eddy Simulation (DES) models. To evaluate the performance of these models, it is essential to use experimental data for flow through filters. However, almost all the available experimental data for pleated filters focused on pressure drop (Feng, 2007; Rebai et al., 2010), not flow field. Because the turbulence intensity in the pleated area is very low, the turbulent characteristics are not used to evaluate the models.

According to the above, the objectives of this investigation are: (1) to measure the flow filed distributions in the pleated filter, (2) to evaluate the performance of various turbulence models for predicting flow fields through pleated filters and (3) to assess the applicability of the selected turbulence models to predict the flow in a combined ESP-pleated filter system. These objectives have led to the results reported in this paper.

Research methods

CFD models

The CFD models assessed in this investigation can be written in a general form as:

$$\rho\frac{\partial\bar{\phi}}{\partial t}+\rho\overline{u_j}\frac{\partial\bar{\phi}}{\partial x_j}-\frac{\partial}{\partial x_j}\left[\Gamma_{\text{eff}}\frac{\partial\bar{\phi}}{\partial x_j}\right]=S_\phi \tag{1}$$

where ϕ is the flow variable, Γ_{eff} the effective diffusion coefficient, S_ϕ the source term, and u_j the velocity component in the j direction, ρ the air density. Table 1 provides the various terms for the models (Zhai et al., 2007) assessed in the present study. In Table 1, u_i is the velocity component in the i direction, k the turbulence kinetic energy, ε the dissipation rate of the turbulence kinetic energy, P the fluid pressure, μ_t the turbulent eddy viscosity, G_k the turbulence production, G_B the generation of turbulence kinetic energy due to buoyancy, and S the rate of strain. σ_k and σ_ε are the turbulent Prandtl numbers for k and ε, respectively. f_1, f_2, and f_μ the damping functions, D and E are additional terms for low-Re model. τ_{ij} is the subgrid stress for the LES model. C_1, C_2, C_3, $C_{\varepsilon1}$, $C_{\varepsilon2}$, C_L, C_η and C_μ are the turbulence constants. The $\overline{v'^2}$ is the fluctuating velocity normal to the nearest wall. The f is part of the $\overline{v'^2}$ source term that accounts for non-local blocking of the wall normal stress, T the turbulence time scale for v2f model.

Table 1 Terms and coefficients for Eq. (1)

	ϕ	Γ_{eff}	S_ϕ	Constants and Coefficients
Standard k-ε (St-kε)	k	$\mu+\mu_\text{t}/\sigma_\text{k}$	$G_\text{k}+G_\text{b}-\rho\varepsilon$	$\mu_\text{t}=\rho C_\mu k^2/\varepsilon; G_\text{k}=\mu_\text{t}S^2; S=(2S_{ij}S_{ij})^{0.5}; G_\text{b}=\beta g_i(\frac{\mu_\text{t}}{\sigma_\text{t}})(\frac{\partial T}{\partial x_j})$
	ε	$\mu+\mu_\text{t}/\sigma_\varepsilon$	$C_1(G_\text{k}+C_3G_\text{b})\varepsilon/k-C_2\rho\varepsilon^2/k$	
Low Re k-ε (LRN)	k	$\mu+\mu_\text{t}/\sigma_\text{k}$	$G_\text{k}-D-\rho\varepsilon$	$\mu_\text{t}=\rho f_\mu C_\mu k^2/\varepsilon; G_\text{k}=\mu_\text{t}S^2; S=(2S_{ij}S_{ij})^{0.5}$
	ε	$\mu+\mu_\text{t}/\sigma_\varepsilon$	$C_1f_1G_\text{k}\varepsilon/k-C_2\rho f_2\varepsilon^2/k+E$	
LES	u_i	μ	$-\frac{\partial p}{\partial x_i}-\frac{\partial \tau_{ij}^S}{\partial x_j}$	$\tau_{ij}\equiv\rho\overline{u_iu_j}-p\overline{u_i}\overline{u_j}; \tau_{ij}-\frac{1}{3}\tau_{kk}\delta_{ij}=-2\mu_\text{t}\overline{S_{ij}}; \overline{S_{ij}}\equiv\frac{1}{2}(\frac{\partial\overline{u_i}}{\partial\overline{x_j}}+\frac{\overline{\partial u_j}}{\partial x_i})$
v2f	k	$\mu+\mu_\text{t}/\sigma_\text{k}$	$G_\text{k}-\rho\varepsilon$	$f-L^2\nabla^2 f=\frac{C_1}{T}(\frac{2}{3}-\frac{\overline{v'^2}}{k})+C_2\frac{G_\text{k}}{\rho k}+5\frac{\overline{v'^2}}{kT}; T=\max(\frac{k}{\varepsilon},6\sqrt{\frac{\mu}{\rho\varepsilon}});$
	ε	$\mu+\mu_\text{t}/\sigma_\varepsilon$	$C_{\varepsilon1}G_\text{k}\varepsilon/k-C_{\varepsilon2}\rho\varepsilon^2/k$	
	$\overline{v'^2}$	$\mu+\mu_\text{t}/\sigma_\text{k}$	$S_{\overline{v'^2}}$	$L=C_\text{L}\max(\frac{k^{1.5}}{\varepsilon},C_\eta(\frac{\mu}{\rho})^{0.75}\varepsilon^{-0.25}); \mu_\text{t}=\rho\min(0.22\overline{v'^2}T,0.09\frac{k^2}{\varepsilon})$

The standard k-ε model (Launder and Splading, 1974) is a two-equation model that can obtain robust, economical, and reasonable results for many engineering flows, although it was developed for high-Reynolds-number flows. Because the model has been widely used, it was selected as a benchmark in this study.

The LRN k-ε models have similar turbulence transport equations but use damping functions (Gürdamar, 2005; Schmidt and Patankar, 2003; Jagadeesh and Murali, 2005). The LRN k-ε models require a very fine grid near the wall, resulting in high computing costs. The LRN models used in the present study include the Abid (AB) (Abid, 1993), Lam-Bremhorst (LB) (Lam and Bremhorst, 1981), Launder-Sharma (LS) (Launder and Sharma, 1974), Yang-Shih (YS) (Yang and Shih, 1993), Abe-Kon-Doh (AKD) (Abe et al., 1994), and Chang-Hsieh-Chen (CHC) (Chang et al., 1995) models. These models differ only in terms of the constants and the expression of damping functions.

The v2f model was developed for low-speed and wall-bounded flow using the fluctuation of normal velocity rather than kinetic energy to calculate the near-wall turbulence-eddy viscosity. This model uses damping functions to limit the fluctuating value of normal velocity in nearly isotropic flow regions in order to obtain accurate results (Durbin, 1991). The model has been recommended for simulating flows in enclosed environments (Zhang et al., 2007). Because of the bounded porous wall flow characteristic in pleated filters, the v2f model may provide good results; therefore, it was also used in this study.

The above models are based on Reynolds-Averaged Navier-Stokes (RANS) equations. LES is an advanced turbulence model that directly calculates large eddies and models small eddies using subgrid-scale models, based on the theory that small-scale eddies can be separated from large-scale eddies. This study tested four widely used subgrid-scale models for LES: the Smagorinsky–Lilly model (SGS) (Smagorinsky, 1963), Dynamic Smagorinsky–Lilly model (DSL) (Germano et al., 1996), Wall-Adapting Local Eddy-viscosity (WALE) model (Nicoud and Ducros, 1999), and Dynamic kinetic energy (Dke) model (Kim, 2004). The first three models use resolved velocity scales and several constants to calculate the subgrid stress, and all of them are based on the assumption that the dissipation of subgrid kinetic energy is equal to the transferred energy from the filter scale. The Dke model solves the transport equation of the subgrid Dke rather than making an assumption.

DES is a hybrid approach combining the LES and RANS models. For DES, the flow field of the near-wall region is resolved by a RANS model, while the fully turbulent region is resolved by LES. This investigation tested three RANS models used in DES: the Spalart–Allmaras model (SA) (Spalart and Allmaras, 1992), Realizable k-ε model (R-kε) (Shih et al., 1995), and SST model (SST) (Menter, 1994).

The present study evaluated these turbulence models for flow through several pleated filters. A commercial CFD software program, ANSYS Fluent (ANSYS Fluent, 2009), was used for the numerical simulations. All the selected turbulence models were available in the CFD software. The SIMPLE algorithm is utilized in the pressure correction equation. The pressure discretization scheme uses the standard first-order upwind, and all the others uses the second-order upwind. For the simulation with LES or DES models, the unsteady simulations were conducted and the time step was 0.001 s.

Experimental setup

Figure 2 shows our experimental test rig for measuring the velocity distributions and turbulence characteristics downstream from a pleated filter. Compressed air was first filtered by a HEPA filter and stored in a constant-pressure tank for supplying clean compressed air to the system. A valve was used to control the airflow rate, which was measured by a flow meter. The air was then divided into four parts through a gas distributor. The four parts entered the experimental channel from the four sides of the channel, which created a uniform flow field in the upstream section of the channel. The experimental

channel was 2 m long with a 200 mm square transverse section. A perforated plate was used to make the flow more uniform. Finally, the gas flowed through the pleated filter that was used for the experiment. The tested filter was rectangular, with a 50 mm pleat length and distance. The pressure drop across the filter was recorded using a differential pressure gauge. The flow velocities behind the filter were measured using a Dantec constant temperature anemometer, and the data were recorded with a computer. The flow velocities behind the filter were measured using a Dantec hot-wire anemometer, and the data were recorded by a computer. The measurement frequency of the anemometer is 2000Hz and the time constant is 0.0005s. The time period of one measurement is 1s. The mean velocity in the experiment is defined as the average value of 2000 samples in 1s. The pressure drop of the pleated filter is measured by a pressure sensor, the sample frequency of which is 10 Hz.

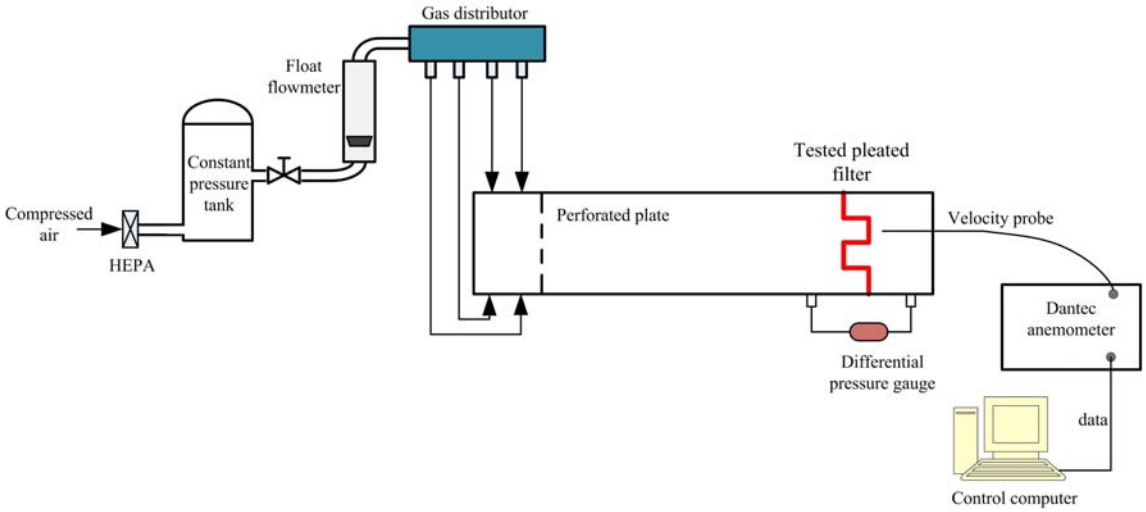

Fig. 2 Diagram of the experimental test rig

Figure 3 shows that the pleated filter was folded with a height of 50 mm and width of 50 mm; its depth extended across the entire width of the channel. The tested pleated filter is quite different from industrial products, which have a higher pleat density. One reason is that a high pleat density would make the pleat distance very small, so that it would be hard to position an anemometer for measuring air velocity. Another reason for making a filter with a short pleat distance is to reduce the laminar effect of the filter media on the flow field. Figure 3 illustrates the measurements that were taken in lines X1 to X4 and Y1 to Y5. Each line had 15–30 measurement points. The measurements were also performed in the Z-direction (along the depth of the filter) along three lines to verify that the flow was two-dimensional. Each measurement was repeated three times.

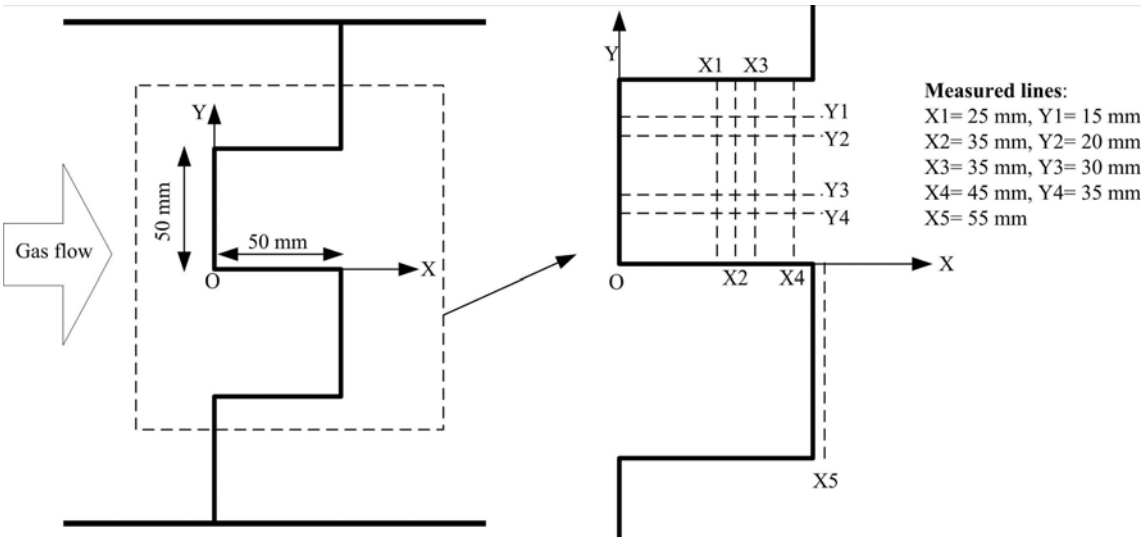

Fig. 3 The geometry of the pleated filter tested and the measurement locations.

The through-plane permeability distribution of filter media may not be uniform, which will result in non-uniform velocity distributions in the filter. This investigation tested the velocity uniformity of four types of common air filter media used for pleated filters by measuring the velocity distributions downstream of the flat filter media. The filter media were polypropylene (PP), glass fiber (GB), polyethylene (PE), and polyester (PET). The size of the flat filter media was 200 mm × 200 mm. The distance between the anemometer and the filter media was 3 mm. Table 2 shows the measured permeability, which can be calculated by the equation:

$$k = \frac{\mu UE}{\Delta P} \tag{2}$$

where U is the measured mean velocity (m/s), E the thickness of measured filter media (m), μ the kinetic viscosity (m^2/s), ΔP the pressure drop across the flat filter media (Pa), and k the through-plane permeability (m^2).

Table 2 The parameters of the filter materials used in the tests

Filter media	Thickness (mm)	Through-plane permeability (m^2)
PP	0.30	8.33×10^{-12}
GB	0.38	1.20×10^{-13}
PE	0.38	4.70×10^{-11}
PET	0.38	3.80×10^{-11}

Results

Preliminary experimental tests

The flow in the channel was measured as one-dimensional along the longitudinal direction before a filter was installed. To investigate the flow uniformity behind a filter, the air velocities in a transverse section were measured carefully with a flat filter, as shown in Figure 4. The uniformity of the filter media was evaluated according to the velocity distribution behind the flat filter. The assessment criterion is the relative root mean square error (RRMSE) of the flow velocities:

$$\mathrm{RRMSE} = \sqrt{\frac{\sum_{1}^{N}(U-\overline{U})^2}{N-1}} / \overline{U} \tag{3}$$

where U is the measured velocity (m/s), N is the number of measured points, and $\overline{U}$ is the average measured velocity.

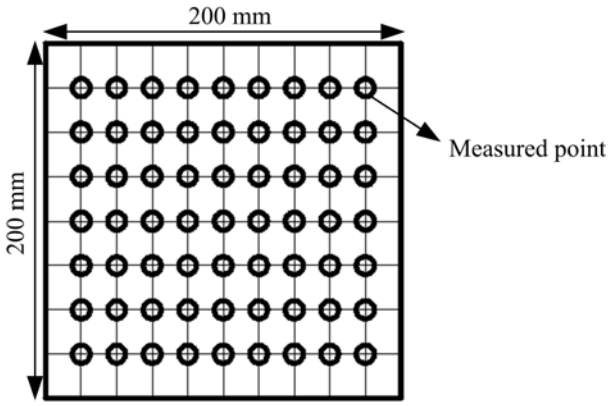

Fig. 4 The measured positions in a transverse section of the experimental channel

The mean velocity in the channel was fixed at 0.13 m/s; the air temperature was about 20°C; and the kinematic viscosity was about 1.46×10^{-5} m^2/s. The measured turbulence intensity in the transverse section was strong, with an average of 15%. The mean velocity, temperature, and turbulence intensity were measured in the channel without a filter.

Figure 5 presents the RRMSE for channel flow without a filter and for the channel flow with the four types of filter media. The results indicate that the channel flow without a filter had a good uniformity with an RRMSE of 8%. The PP and GB media had very homogeneous structures, which can be easily modeled as porous media in numerical simulations. Meanwhile, the structures of the PE and PET media resulted in non-homogeneous flows with an RRMSE higher than 20%, which would be difficult to simulate numerically. The pleated filter used in the experiment was made by hand. Because the GB media were somewhat soft for the hand-made process, this investigation selected the PP media for our flow tests.

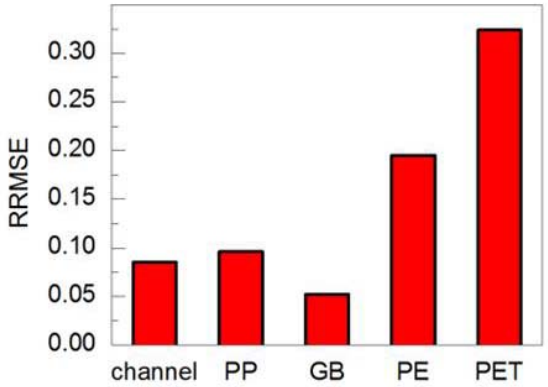

Fig. 5 Non-uniformity of the channel flow without and with the four types of filter media

Velocity measurements

After the pleated filter with the PP media had been installed in the test rig, this investigation measured

the velocity distribution in lines X1 to X5 and Y1 to Y5. The one-dimensional velocity component along the longitudinal direction was measured. Figure 6 shows the x-velocity component for lines X1, Y4, and X5, where the error bars represent the differences among the three measurements. The repeatability of the measurements was quite good. The x-velocity distribution along line X1, as shown in Figure 6(a), was bimodal with two peaks, and the x velocity at the middle point was about 70% of the peak velocity. Figure 6(b) shows the relationship between the x velocity and the x position to be approximately linear, and the relatively uniform air flow across the filtration media caused a linear increase in the x velocity. The measured x-velocity profiles for X2 and X3 had a similar shape to that of X1, and those for Y1, Y2, and Y3 had a similar shape to that of Y4 but with different values, although they are not shown here. Figure 6(c) shows the measured x-velocity profile of X5, with a very uniform distribution. The distance between the filter surface and line X5 was 2 mm, and the x-velocity at line X5 was approximately equal to the filtration velocity. Figure 7 explains why the x-velocity profile of X1 line is bimodal. Because of high pressure drop value of filter media, the filtration velocity along the filter media is uniform and perpendicular to the filter media surface. For the x-velocity profile of line X1, the value of x-velocity increases from point A to point B because of the y-velocity component of the air flow though the filter media and the value of x-velocity decreases from point B to point C because of the collision between air flow from upper and down filter media.

The average filtration velocity can be calculated by equation:

$$v_f = v \times \frac{A_s}{A_f} \tag{4}$$

where A_s is the area of the channel's transverse section, A_f is the total area of the filter surface, v is the upstream velocity before the filter, and v_f is the filtration velocity. The average filtration velocity calculated for line X5 was 0.072 m/s, which was very close to the experimentally measured velocity of 0.074 m/s.

The measured pressure drop for this pleated filter was 470 Pa when the channel velocity was 0.13 m/s. The pleated filter experienced a slight deformation with the pressure drop. If this investigation had increased the channel velocity and pressure loss, the pleated filter may have had a serious deformation or even been destroyed. The iron grid commonly used in industrial filters would increase structural strength in test filters.

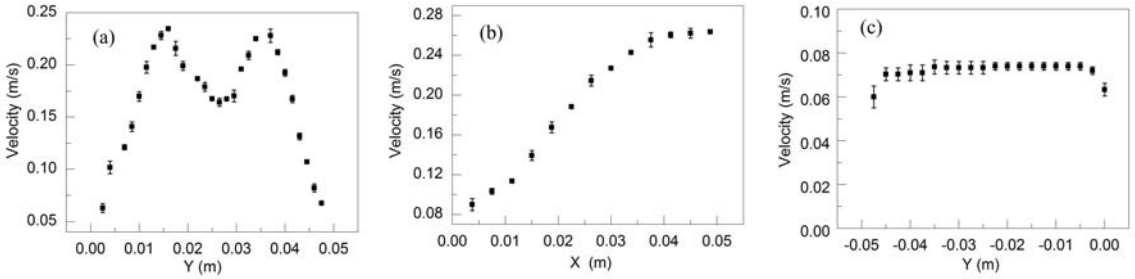

Fig. 6. The measured x-velocity profile along (a) line X1, (b) line Y4, and (c) line X5

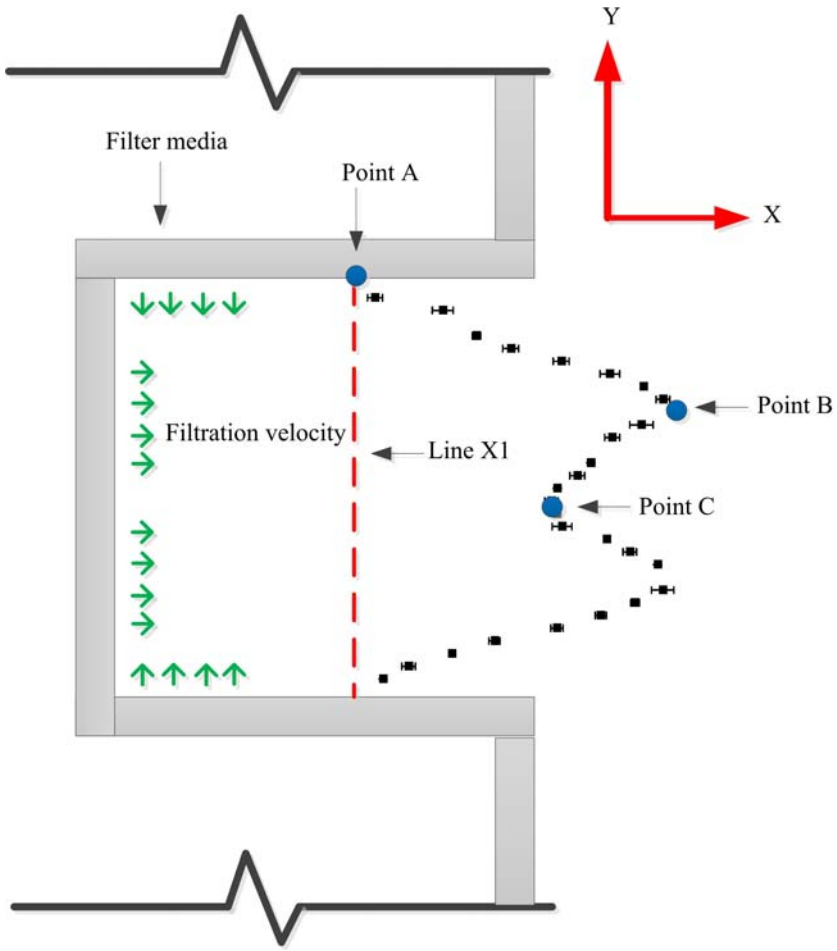

Fig. 7 The filtration process in pleated filter and measured x-velocity profile along line X1.

Numerical simulations of the pressure drop through the filter

All the CFD models shown in Table 1 were used to calculate the pressure drop through the filter, but not all the results are presented here because of the limited space available in this paper. Only the LES (SGS), DES (SA), LRN (LS), standard *k-ε,* and v2f models are presented because they are widely used. For the simulation with LES or DES models, the unsteady simulations are conducted and the time step is 0.001s. During the simulation, all the quantities were averaged every 1000 time-steps. The model predictions presented in the following figures are the values of the final average. The calculation flow time for LES and DES cases was about 17 second and 15 second, respectively. Their times ensured that the final flow reached the steady statues.

Figure 8 shows the pressure drop calculated by these turbulence models. All the models provide similar and satisfactory results, but this does not imply that these models can accurately predict the performance of the pleated filter. The total pressure drop of the pleated filter is the sum of the pressure drop across the filter media and the pressure drop caused by the pleated channel. The pleated filter used in the experiment was made of PP filter media with a high resistance and permeability of 8.33×10^{-13} m^2. Because of the high filter media resistance and low filtration velocity, the pleated channel pressure drop was negligible as compared to that of the filter media. The total pressure drop of the test filter was determined from the filter media rather than the detailed flow field around the filter. Hence, the use of pressure drop as a criterion for assessing different turbulence models could be misleading in this case.

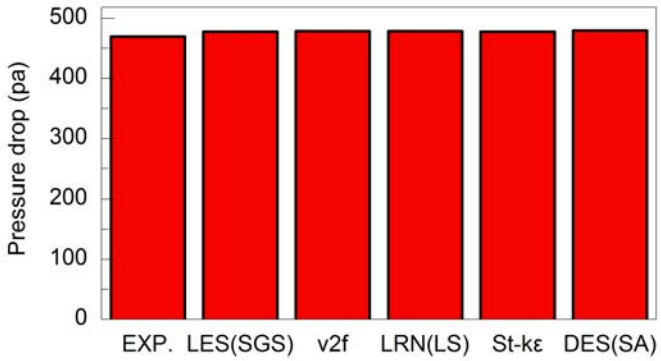

Fig. 8 Comparison of the pressure drop through the filter as predicted by various CFD models with the experimental data.

Therefore, this investigation simulated the cases from Rebai et al. (2010), and their measured pressure drop data were used to validate the CFD models. Table 3 summarizes the pleated filter characteristics and the boundary conditions used by Rebai et al. (2010), as compared with the parameters used in our experiment. In Rebai's case, the filter media resistance was not high, such that the pressure drop through the pleat channel was important. The ratio of the filter media pressure drop to the total filter pressure drop was 0.34, as compared to near zero in the present study.

Table 3 Comparison of filter media and test conditions used in Rebai et al. (2010) and the present study.

Case	Pleat width (mm)	Pleat height (mm)	Permeability (m^2)	Media thickness (mm)	Duct face velocity (m/s)
Rebai et al.	12.5	51	3.57×10^{-10}	1.45	2.400
Present study	50	50	8.33×10^{-12}	0.30	0.130

Figure 9 shows the simulated pressure drop as obtained by the CFD models for Rebai's case. The LES (SGS) and DES (SA) models can provide an acceptable pressure drop, as compared with the experimental data from literature. Most of the RANS models performed poorly in predicting the pressure drop, although many of the results are not presented in Figure 9. The v2f model can successfully predict the pressure drop, perhaps because the model accurately predicts the normal stress on the filter, which is an important feature of the pleated filter flow field. Because the pressure drop through the pleat channel was important in this case, prediction of the detailed flow field in the filter channel was crucial in predicting the total filter pressure drop. Because the flow was complex, advanced models, such as LES and DES, were capable of predicting the flow as well as the pressure drop, but most of the RANS models were not.

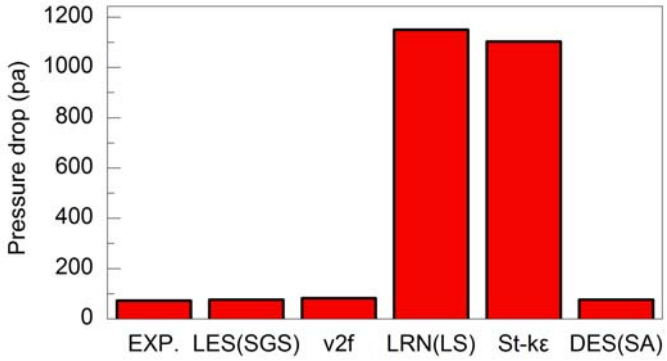

Fig. 9 Comparison of the pressure drop as predicted by various CFD models with the experimental data from Rebai et al. (2010).

Numerical simulations of the flow field

It is difficult to thoroughly evaluate the performance of turbulence models for a pleated filter using pressure drop as the only criterion because it is a lump sum value. The models should be also evaluated using the flow field data around the filter.

Figures 10-11 compare the velocity predicted by different CFD models with the experimental data in lines X1, X3, Y1, and X5. Figure 10(a) shows that the LES (SGS) model with the Smagorinsky-Lilly subgrid-scale model can successfully predict the velocity profile. The DES (SA) model provided good agreement with the experimental results. The v2f models provided acceptable velocity results, but slightly underestimated the peak value. The v2f model has been widely adopted for flow simulations in enclosed spaces using the fluctuation of normal velocity rather than the kinetic energy to calculate near-wall turbulence eddy viscosity. It is suitable for modeling low-speed and near-wall flow, such as the relatively low duct velocity and the complex porous wall in the pleated filter. The LRN (LS) model and the standard k-ε model had a slightly poorer performance than the v2f model. Figure 10(b) shows similar results for line X3, but the LRN (LS) and standard k-ε models performed very poorly for this location.

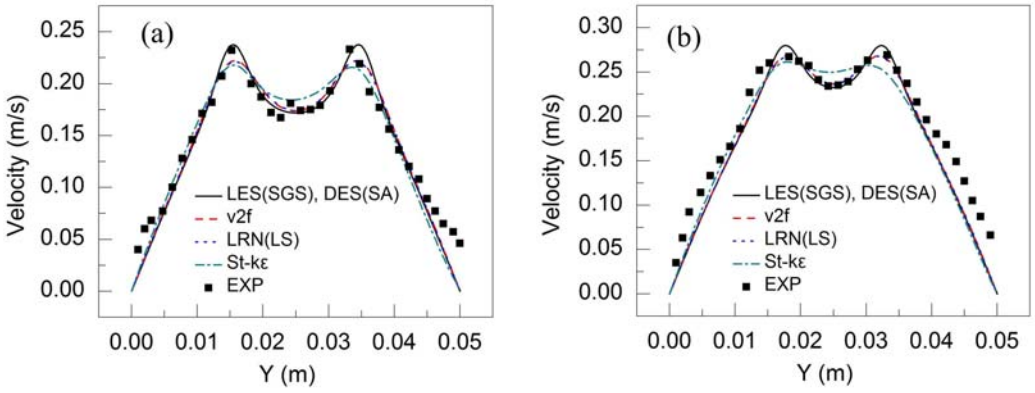

Fig. 10 The simulated and measured velocity profiles along (a) line X1 and (b) line X3.

Figure 11 further compares the simulated and measured velocity profiles along lines Y1 and X5. None of the models produced an accurate velocity profile, although the results are not too bad. It was surprising that the LES (SGS) and DES (SA) models did not perform better than the other models. The velocity distribution along line X5 was nearly constant because the distance between the measured positions and the

media surface was only 2 mm. The velocity was close to the filtration velocity, which was determined by the pressure drop across the filter media.

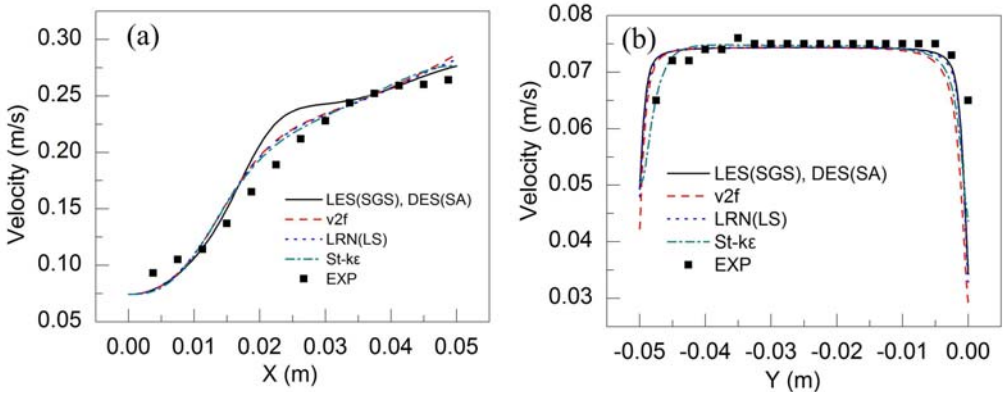

.

Fig. 11 The simulated and measured velocity profiles along (a) line Y1 and (b) line X5.

Rebai et al. (2010) developed a theoretical method to calculate the filtration velocity along the filter surface and the pressure drop of the pleated filter. Figure 12 indicates that the velocity distributions predicted by the LES (SGS), DES (SA), and v2f models are in good agreement with that calculated by the theoretical model. As shown in Figure 9, the pressure drop across the filter is also predicted well by these models. In contrast, the St-kε model and LRN (LS) model gave unacceptable predictions. The filter in these cases had a relatively high pleat density and low permeability, resulting in a low pressure drop across the filter media but a high structural pressure drop in the air channel. The incorrectly predicted flow field would have a significant effect on the pressure drop, as depicted in Figure 9.

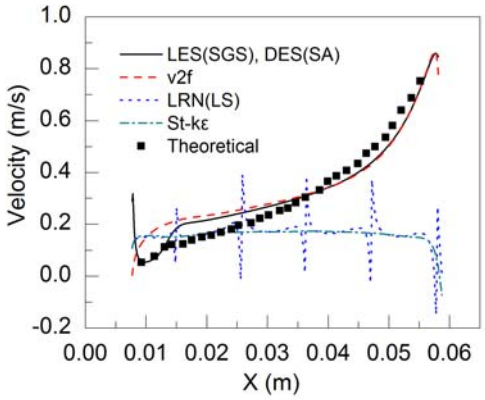

Fig. 12 The filtration velocity distribution along the filter surface as determined by different models for Rebai's case.

Discussion

The LES (SGS), DES (SA), and v2f models provided acceptable pressure drop and velocity distributions for a pleated filter. However, the LES model required a very fine mesh and was computationally demanding. The computing time for the v2f model was the shortest among the validated models, but the initial flow field used for the computation was important for the convergence speed. The DES (SA) model was a stable model with acceptable computing costs. This investigation also tested LES with different subgrid scale models, including LES (WALE) and LES (Dke); DES with different RANS models, including DES (SST) and DES (R-kε); and five other LRN models. Different LES and DES

models successfully predicted the flow velocity profiles with similar accuracy, but the DES (R-kε) model failed. A unique characteristic of the R-kε model is that it ensures that the normal Reynolds stresses are positive, which is suitable for flows with high Reynolds numbers, strong streamline curvatures, vortices, and rotations. This characteristic was not necessary for transitional flow in pleated filters. The performance of the other five LRN models was not as good as the LES and DES models because the two peak values were not well predicted, although the predictions may be acceptable in engineering applications.

In a pleated filter system that incorporates an ESP, the flow field is coupled with an electric field generated in the ESP, called the electro-hydrodynamic field (Yabe et al., 1978). The influence of the electric field on the flow field is taken into account by adding an electric force term to the source term when Eq. (1) represents the momentum equations (Long and Yao, 2010):

$$S_\phi \text{ (new)} = S_\phi + F_{ci} \tag{5}$$

where F_{ci} is the electric body force (N/m^3).

As LES is very time-consuming, this investigation used only the DES, v2f, and standard k-ε models to predict the electro-hydrodynamic flow. Figure 13 compares the velocity profiles predicted by these models with the experimental data (Kallio and Stock, 1992). The performance of the DES models was the best, and the v2f model was also very good. The standard k-ε model had poor performance, as it again failed to yield an acceptable profile.

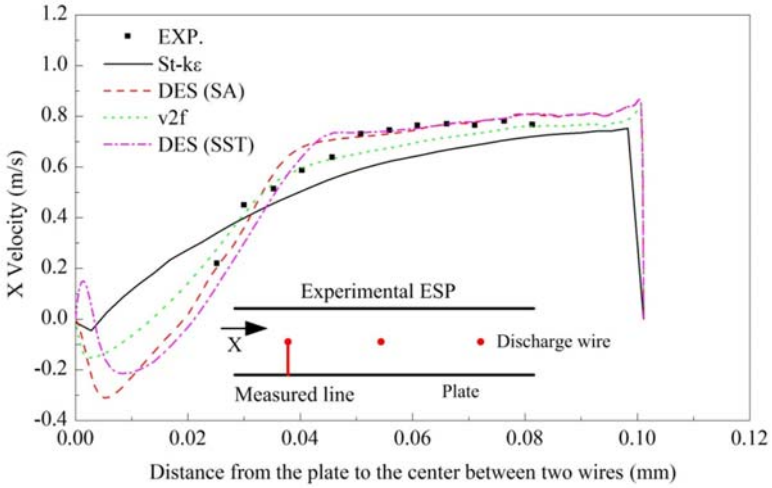

Fig. 13 Comparison of the velocity profiles as predicted by different turbulence models with the experimental data from Kallio and Stock (1992).

Figure 14 shows a hybrid system consisting of an electrostatic precipitator (ESP) and a pleated filter. The radius of the discharge wire is 1 mm and the length of the collection plate is 1524 mm, while the wire to plate distance is 1143 mm. The thickness of the pleated filter media is 0.3 mm and the media permeability is 1E-11 (m^2). The pleat count density is 200 N/m. The inlet velocity is 0.8 m/s and average filtration velocity for pleated filter is 0.02 m/s. The finite volume method is used to solve the governing equations of the electric potential and the space density (Long et al. 2009). Based on the conclusions above, the flow field in this hybrid electrostatic filtration system is simulated by using the DES-SA turbulence model. The filter media is modeled as the porous media. Figures 15(a) and (b) show the normalized predictions of electric potential and space charge density. The simulated electric field is validated by the measured data in literature (Penney and Matick, 1960). Figure 15(c) shows the relative static pressure distribution in the hybrid system. The measured pressure drop of the pleated filter is 145 Pa. The DES

model prediction agrees well with this value. In the transverse direction, the pressure is evenly distributed. Based on these results, the particle deposition characteristics in this hybrid system can be studied, which is useful for the optimal design of the hybrid system.

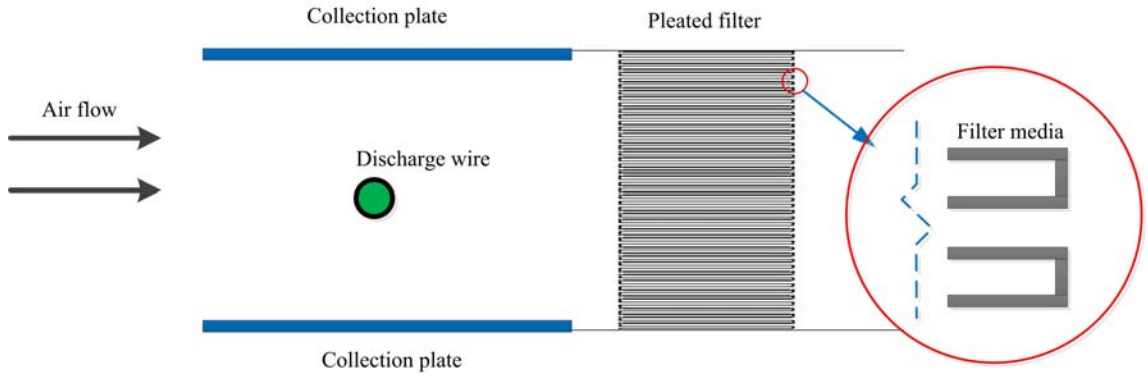

Fig. 14 The layout of the hybrid electrostatic filtration system.

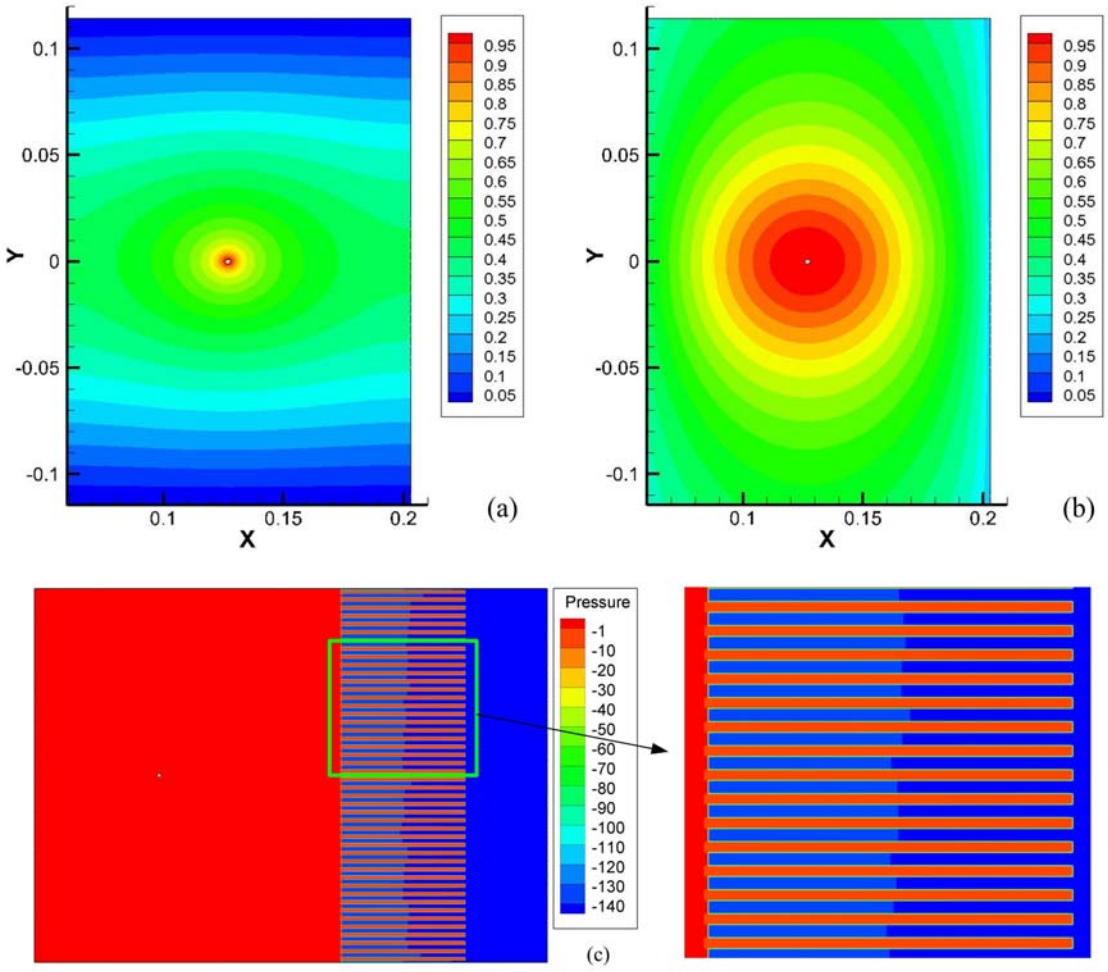

Fig. 15 The simulated results: (a) the normalized electric potential; (b) the space charge density; (c) the pressure distribution in the hybrid electrostatic filtration system.

Conclusion

This investigation evaluated the performances of several turbulence models for predicting the pressure

drop and flow field in pleated filter systems. The evaluation used experimental data for the pressure drop through a pleated filter from the literature and the measured flow field in an experimental pleated filter. By assessing the standard k-ε model, six low-Reynolds-number models, the v2f model, three LES models, and three DES models, this investigation found that the v2f, LES, and DES (Spalart–Allmaras) model can accurately predict the pressure drop and the flow filed through a pleated filter. The other models failed in predicting such a flow because of the high-Reynolds-number assumption used in the standard k-ε model or the lack of a mechanism for solving the special flow characteristics in the filter. Among the useable models, the LES requires the highest computation time. Besides, for the flow in the electrostatic precipitator, the DES (Spalart–Allmaras) model has better performance than the v2f model. Finally, the DES (Spalart–Allmaras) model is recommended for simulating the pressure drop and airflow through a pleated filter both with and without an electrostatic precipitator.

Acknowledgements

The research presented in this paper was financially supported by the National Basic Research Program of China (the 973 Program) through Grant No. 2012CB720100 and the National Natural Science Foundation of China though Grant No. 51106105.

References

Abe, K., Kondoh, T., Nagano, Y., 1994. A new turbulence model for predicting fluid flow and heat transfer in separating and reattaching flows – 1. Flow field calculations. Int .J. Heat and Mass Transfer. 37(1): 139 -151.

Abid, R., 1993. Evaluation of two-equation turbulence models for predicting transitional flows. International Journal of Engineering Science. 31: 831-840.

ANSYS Fluent. 2009. ANSYS Fluent 12.0 Documentation. ANSYS Fluent Inc., Lebanon, NH.

Chang, K.C., Hsieh, W.D., Chen, C.S., 1995. A modified low-Reynolds-number turbulence model applicable to recirculating flow in pipe expansion. Journal of Fluid Engineering, 117: 417-423.

Chen, D. R., Pui, D. Y. H., Liu, B. Y. H., 1995. Optimization of pleated filter designs using a finite-element numerical model. Aerosol Science and Technology, 23 (4): 579–590.

Chio, Chia-Pin, Liao Chung-Min, 2008. Assessment of atmospheric ultrafine carbon particle-induced human health risk based on surface area dosimetry. Atmospheric Environment, 42(37): 8575-8584.

Clausen, G.. 2004. Ventilation filters and indoor air quality: a review of research from the International Centre for Indoor Environment and Energy. Indoor air , 14 (7) :202-207.

Croxford, B., Tham, K.W., Young, A., Oreszczyn, T., Wyon, D., 2000. A study of local electrostatic filtration and main pre-filtration on airborne and surface dust levels in air-conditioned office premises. Indoor Air, 10(3): 170-177.

Durbin, P.A., 1991. Near-wall turbulence closure modeling without “damping functions”. Theoretical and Computational Fluid Dynamics, 3(1):1-13.

Feng, Z.Y., 2007. An experimental study of the relationship between resistance and structure of a high efficiency particulate air filter. M.S. Thesis, Tsinghua University, China.

Fotovati, S., Tafreshi, H.V., 2011. Modeling instantaneous pressure drop of pleated thin filter media during dust loading. Chemical Engineering Science, 66(18); 4036–4046.

Fotovati, S., Tafreshi, H.V., 2012. A macroscale model for simulating pressure drop and collection efficiency of pleated filters over time. Separation and Purification Technology, 98(19): 344–355.

Gallimberti, I., 1998. Recent advancements in the physical modelling of electrostatic precipitators. Journal of Electrostatics, 43(4): 219-247.

437 Germano, M., Piomelli, U., Moin, P., Cabot, W.H., 1996. Dynamic subgrid-scale eddy viscosity model. In
438 Summer Workshop, Center for Turbulence Research, Stanford, CA.
439 Gürdamar, E., 2005. Adaptation of turbulence models to a Navier-Stokes solver. M.S. Thesis, Middle East
440 Technical University, Republic of Turkey.
441 Hocking M., 2000. Passenger aircraft cabin air quality: trends, effects, societal costs, proposals.
442 Chemosphere, 41: 603–15.
443 Huang, R., Agranovski, I., Pyankov, O., Grinshpun, S., 2008. Removal of viable bioaerosol particles with a
444 low-efficiency HVAC filter enhanced by continuous emission of unipolar air ions. Indoor air, 18(2):
445 106-112.
446 Jagadeesh, P., Murali. K., 2005. Application of low-re turbulence models for flow simulations past
447 underwater vehicle hull forms. Journal of Naval Architecture and Marine Engineering, 2(1):41-54.
448 Kallio, G.A., Stock, D. E., 1992. Interaction of electrostatic and fluid dynamic fields in wire-plate
449 electrostatic precipitators. J. Fluid Mech., 240: 133-166.
450 Kim, S.E., 2004. Large eddy simulation using unstructured meshes and dynamic subgrid scale turbulence
451 models. Technical Report AIAA-2004-2548, American Institute of Aeronautics and Astronautics, 34th
452 Fluid Dynamics Conference and Exhibit.
453 Lam, C.K.G., Bremhorst, K., 1981. A Modified Form of the k-e Model for predicting wall turbulence. J. of
454 Fluids Engineering, 103: 456-460.
455 Launder, B., Sharma, B., 1974. Application of the energy dissipation model of turbulence to the calculation
456 of flow near a spinning disc, Lett. Heat and Mass transfer, 1: 131-138.
457 Launder, B.E., Spalding, D.B., 1974. The numerical computation of turbulent flows. Computer Methods in
458 Applied Mechanics and Engineering, 3(2): 269–289.
459 Liu,W., Long, Z.W., Chen Q.Y., 2012. A procedure for predicting pressure loss coefficients of duct fittings
460 using computational fluid dynamics (RP-1493). 18(6); 1168-1181.
461 Long, Z.W., Yao, Q., 2010. Evaluation of various particle charging models for simulating particle dynamics
462 in electrostatic precipitators. Journal of Aerosol Science, 41(7): 702-718.
463 Long, Z.W., Yao, Q., 2012. Numerical simulation of the flow and the collection mechanism inside a scale
464 hybrid particulate collector. Powder Technology, 215-216: 26-37.
465 Mangili A, Gendreau M A. 2005. Transmission of infectious diseases during commercial air travel. Lancet,
466 365: 989–96.
467 Menter, F.R., 1994. Two-equation eddy-viscosity turbulence models for engineering applications. AIAA
468 Journal, 32(8):1598–1605.
469 Morawska, L., Agranovski, V., Ristovski, Z., Jamriska, M., 2002. Effect of face velocity and the nature of
470 aerosol on the collection of submicrometer particles by electrostatic precipitator. Indoor air, 12(2):
471 129-137.
472 Nicoud, F., Ducros. F., 1999. Subgrid-Scale Stress modelling based on the square of the velocity gradient
473 tensor. Flow, Turbulence, and Combustion, 62(3): 183-200.
474 Park, J. H., Yoon, K.Y., Hwang, J., 2011. Removal of submicron particles using a carbon fiber
475 ionizer-assisted medium air filter in a heating, ventilation, and air-conditioning (HVAC) system.
476 Building and Environment, 46(8): 1699-1708.
477 Park, J. H., Yoon, K.Y., Kim, Y.S., Byeon., J. H., Hwang, J., 2009. Removal of submicron aerosol particles
478 and bioaerosols using carbon fiber ionizer assisted fibrous medium filter media. Mechanical Science
479 and Technology, 23(7): 1846~1851.
480 Pope III, C.A., Burnett, R.T., Thun, M.J., et al., 2002. Lung cancer, cardiopulmonary mortality, and

481 long-term exposure to fine particulate air pollution. Journal of the American Medical Association,
482 287(9): 1132–1141.
483 Rebai, M., Prat, M., Meireles, M., Schmitz, P., Baclet, R., 2010. A semi-analytical model for gas flow in
484 pleated filters. Chemical Engineering Science, 65(9): 2835–2846.
485 Schmid, H.J., Stolz, S., Buggisch, H., 2002. On the modelling of the electro-hydrodynamic flow field in
486 electrostatic precipitators. Flow, Turbulence and Combustion, 68(1): 63-89.
487 Shih, T.H., Liou, W.W., Shabbir, A., Yang, Z., Zhu., J., 1995. A new k-eddy-viscosity model for high
488 Reynolds number turbulent flows - model development and validation. Computers Fluids,
489 24(3):227–238.
490 Skulberg, K.R., Skyberg, K., Kruse, K., Eduard, W., Levy, F., Kongerud, J., Djupesland, P., 2005. The
491 effects of intervention with local electrostatic air cleaners on airborne dust and the health of office
492 employees. Indoor air,15(3):152-159.
493 Schmidt, R.C., Patankar, S.V., 1988. Two-equation low-Reynolds-number turbulence modeling of
494 transitional boundary layer flows characteristic of gas turbine blades. NASA contractor report 4145.
495 Smagorinsky, J. 1963. General circulation experiments with the primitive equations. I. The basic
496 experiment. Monthly Weather Review, 91: 99–164.
497 Song, S., Lee, K., Lee, Y.M., Lee J.H., Lee, S.I., Yu, S.D., Paek, D., 2011. Acute health effects of urban fine
498 and ultrafine particles on children with atopic dermatitis. Environmental Research, 111(3), 394-399.
499 Spalart, P., Allmaras, S., 1992. A one-equation turbulence model for aerodynamic flows. Technical Report
500 AIAA-92-0439, American Institute of Aeronautics and Astronautics.
501 Subrenat, A., Bellettre, J., Cloirec, P.L., 2003. 3-D numerical simulations of flows in a cylindrical pleated
502 filter packed with activated carbon cloth. Chemical Engineering Science, 58 (22): 4965–497.
503 Yabe, A., Mori, Y., Hijikata, K., 1978. EHD study of the corona wind between wire and plate electrodes.
504 AIAA J., 16:340-345。
505 Yang, Z., Shih, T.H. 1993. New time scale based k-ε model for near-wall turbulence. AIAA Journal. 31(7) :
506 191 – 1198.
507 Zhang, Z., Zhang, W., Zhai, Z., Chen. Q. 2007. Evaluation of various turbulence models in predicting
508 airflow and turbulence in enclosed environments by CFD: Part-2: comparison with experimental data
509 from literature. HVAC&R Research, 13(6): 871-886.
510 Zhai, Z., Zhang, Z., Zhang, W., Chen, Q., 2007. Evaluation of various turbulence models in predicting
511 airflow and turbulence in enclosed environments by CFD: Part-1: summary of prevalent turbulence
512 models. HVAC&R Research, 13(6): 853-870.
513 Zuraimi, M.S., Tham, K.W., 2009. Reducing particle exposures in a tropical office building using
514 electrostatic precipitators. Building and Environment, 44(12): 2475-2485.